

Submitted to: *Phys. Med. Biol.*

# Generalization and specialization of multiple scattering theory for Gaussian beam model of heavy charged particles in radiotherapy

Nobuyuki Kanematsu

Department of Accelerator and Medical Physics, Research Center for Charged Particle Therapy, National Institute of Radiological Sciences, 4-9-1 Anagawa, Inage-ku, Chiba 263-8555, Japan

E-mail: nkanemat@nirs.go.jp

**Abstract.** Theories on multiple scattering of charged particles are reorganized to construct an accurate, efficient, and simple Gaussian-beam transport model for radiotherapy with protons and heavier ions. The Highland formula for scattering angle is modified to a scattering power formula to be used within the Fermi-Eyges theory for particle transport in the presence of heterogeneity. Semi-analytic formulas for scattering displacements in homogeneous matter are also derived for arbitrary ions. The resultant scattering angles and displacements for protons, helium ions, and carbon ions excellently agreed with other experimental and theoretical studies at a level of 1–2%. The present formulation will provide a general solution in a specific field of radiotherapy with heavy charged particles.

PACS numbers: 11.80.La , 29.27.Eg, 87.53.Kn, 87.55.kd

## 1. Introduction

Heavy charged particles such as protons and heavier ions are naturally hard to bend until they stop at a certain depth in matter with the Bragg peak in dose, which is precisely controllable by energy adjustment. Such an intrinsic three-dimensional targeting capability makes the radiation ideal for cancer therapy (Chu *et al* 1993). The targeting precision would degrade due to scattering by atomic electric fields in matter, which have been theoretically and experimentally studied for a long time (Rutherford 1911, Rossi and Greisen 1941, Eyges 1948, Bethe 1953, Hanson *et al* 1951, Bichsel 1958, Highland 1975, Wong *et al* 1989, Gottschalk *et al* 1993).

In treatment planning, a field of charged particles is usually modeled as a set of Gaussian pencil beams that are physically approximate to the reality, algorithmically efficient for good localization nature, and computationally easy and fast with the standard math library (Hong *et al* 1996, Kanematsu *et al* 1998, 2006, 2008a, 2008b, Deasy 1998, Sandison *et al* 2000, Hollmark *et al* 2004, Ciangaru *et al* 2005, Safai *et al* 2008). Although all those implementations are based on the same algorithmic principle, employed physical models for scattering calculation vary in several ways. General theory of electromagnetic interactions may be specialized for convenience, while empirical models may be generalized for wider applicability, to construct an optimum framework for scattering calculation in radiotherapy.

A reasonable tolerance to spatial errors in high-precision radiotherapy may be one millimeter in absolute position or one percent in relative size that would be about the limits in beam control with respect to a nonrigid target in human body. Since the size of scatter is typically a few to several millimeters, the accuracy better than ten percent would always fulfill the one-millimeter tolerance. The present work is motivated to optimize the physical and computational models against such tolerances. We first review the theories of multiple scattering to identify the most appropriate approach, delineate room for improvement, address a reasonable solution, and discuss the results of the modified and extended formulation.

## 2. Materials and methods

### 2.1. Historical review

**2.1.1. Rutherford scattering** Elastic scattering of a charged particle by a static point-like nucleus, Rutherford scattering, is one of the elementary processes of charged-particle interactions. Rutherford (1911) formulated the differential cross section as

$$\frac{d\sigma}{d\Omega} = \left( \frac{\alpha\hbar c}{2} \frac{z}{pv} Z \right)^2 \left( \sin \frac{\theta}{2} \right)^{-4}, \quad (1)$$

where  $\alpha\hbar c \approx 1.44 \text{ MeV} \cdot \text{fm}$  is a physical constant,  $z$ ,  $p$ , and  $v$  are the charge in units of proton charge  $e$ , the size of momentum, and the speed of the projectile particle, and  $Z$  is charge in  $e$  of the target nucleus. This *single scattering* is enhanced in the forward direction with dependence  $\sim 1/\theta^4$ .

**2.1.2. Fermi-Rossi theory** In matter, a particle receives *multiple scattering* of a large number of single-scattering processes by nuclei with electric field screened by orbital electrons. Fermi developed a theory of multiple scattering (Rossi and Greisen 1941) in the form of

$$\frac{d\overline{\theta^2}}{dx} = \frac{1}{2} \left( \frac{E_s z}{pv} \right)^2 \frac{1}{X_0} \quad \text{or} \quad \overline{\theta^2} = \frac{1}{2} \int_0^x \left( \frac{E_s z}{pv} \right)^2 \frac{dx'}{X_0}, \quad (2)$$

where  $\overline{\theta^2}$  is the variance of projected scattering angle,  $x$  is the position in the forward direction,  $E_s = m_e c^2 \sqrt{4\pi/\alpha} \approx 21.2 \text{ MeV}$  is a constant energy, and  $X_0$  is the material-specific radiation length in which a high energy electron would lose its kinetic energy by bremsstrahlung down to  $1/e$  in average (Yao *et al* 2006). The kinematic factor  $z^2/(pv)^2$  is naturally common to the Rutherford scattering cross section formula (1). Since bremsstrahlung is caused by an electron scattered by a nucleus, number of single-scattering processes should be also proportional to radiative path length  $\int dx'/X_0$ . The relation  $\overline{\theta^2} \propto \int dx'/X_0$  is thus compliant to the central-limit theorem for a large number of small fluctuations in statistics.

The Fermi-Rossi formula is computationally very convenient with material properties encapsulated in the  $X_0$  and decoupled to the particle kinematics. However, it totally ignores the single-scattering contributions at large angles that may linearly increase with the radiative path length. Consequently, Gaussian beam models with variance of this  $\overline{\theta^2}$  may not be very accurate.

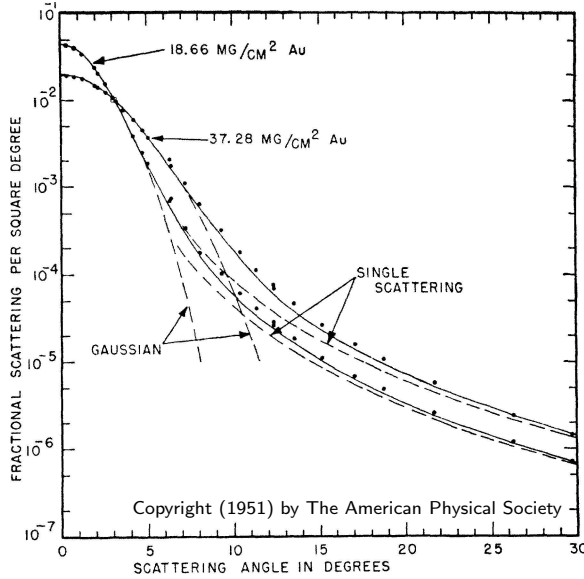


**Figure 1.** Angular distribution of electrons from thick and thin gold foils by Hanson *et al* (1951). The markers and the solid lines represent their measurement and the Molière theory. The dashed lines represent either the best-fit Gaussian distributions at small angles or the single scattering contributions at large angles.

*2.1.3. Molière theory* Molière developed a theory to rigorously address the situation of multiple scattering with single scattering contributions and formulated an analytical expression of the angular distribution for a particle interacting with individual atomic components of the target (Bethe 1953). The Molière distribution consists of Gaussian main part for multiple scattering at small angles and the  $1/\theta^4$ -tail for single scattering at large angles, experimentally verified as shown in figure 1. Such a long tail is undesirable for dose convolution algorithms because it would contribute little in dose, makes computation inefficient (Kanematsu *et al* 2008a), and invalidates the pencil beam model in the presence of heterogeneity (Kanematsu *et al* 2008b). In fact, an approximate Gaussian formulation by Hanson *et al* (1951) is used more often than the original Molière distribution (Deasy 1998, Ciangaru *et al* 2005) though the complexity of the theory would discourage its direct use in demanding applications such as treatment planning.

*2.1.4. Highland formula* Highland (1975) introduced a logarithmic correction term with an optimized energy constant to the Fermi-Rossi formula for better agreement with the Molière-Hanson angles, which was further generalized by Gottschalk *et al* (1993) for a thick target as

$$\sigma_{\theta}(x) = \left(1 + \frac{1}{9} \lg \frac{x}{X_0}\right) \sqrt{\int_0^x \left(\frac{14.1 \text{ MeV } z}{pv(x')}\right)^2 \frac{dx'}{X_0}}, \quad (3)$$

where  $x$  is stated as the thickness of the target,  $\lg = \log_{10}$  is the common logarithmic function, and  $\sigma_{\theta} = \sqrt{\langle \theta^2 \rangle}$  is the rms projected scattering angle. The Highland formula has been experimentally verified to be accurate (Wong *et al* 1989, Gottschalk *et al*

1993) and has been commonly applied to practical dose distribution calculations for proton radiotherapy (Hong *et al* 1996, Kanematsu *et al* 1998, 2006, Safai *et al* 2008).

*2.1.5. Ionization energy loss* For semi-relativistic charged particles for radiotherapy, the Bethe formula for stopping power

$$S = -\frac{dE}{dx} = 4\pi N_A r_e^2 m_e c^2 \frac{n_e}{N_A} z^2 \left[ \frac{c^2}{v^2} \ln \frac{2 m_e c^2 v^2}{I (c^2 - v^2)} - 1 \right] \quad (4)$$

accurately describes its stopping process (Yao *et al* 2006), where Avogadro's number  $N_A$ , classical electron radius  $r_e$ , electron mass  $m_e$ , and speed of light  $c$  are physical constants, electron density  $n_e$  and mean excitation energy  $I$  are material properties, and kinetic energy  $E$ , mass  $m$ , and speed  $v$  are particle parameters with kinematic relations  $pc = \sqrt{E^2 + 2mc^2E} = (E + mc^2)v/c$ .

The stopping-power ratio  $\rho_S$  of body tissue, that is the ratio of the stopping power of the material to that of water, is usually estimated from x-ray attenuation in computed tomography (Kanematsu *et al* 2003). For physical devices in beam-delivery systems, the stopping-power ratio may be approximated to

$$\rho_S = \frac{S}{S_w} \simeq \frac{n_e/N_A}{0.5551 \frac{\text{mol}}{\text{cm}^3}} \frac{\ln(2 m_e c^2 / I) - 0.5}{9.020}, \quad (5)$$

representing the semi-relativistic speeds in those upstream devices by  $v^2 = 0.5 c^2$ , which is also valid for downstream devices made of materials with the mean excitation energy close to that of water ( $I = 75$  eV) regardless of the speed.

*2.1.6. Fermi-Eyges theory* Probability density of a particle with transverse position  $y$  and angle  $\theta$  in a Gaussian beam is described by phase-space distribution

$$F(y, \theta) = \frac{1}{2\pi} \left( \overline{y^2 \theta^2} - \overline{y\theta} \right)^{-\frac{1}{2}} \exp \left( -\frac{1}{2} \frac{\overline{\theta^2} y^2 - 2 \overline{y\theta} y\theta + \overline{y^2} \theta^2}{\overline{y^2 \theta^2} - \overline{y\theta}^2} \right), \quad (6)$$

which is characterised by angular variance  $\overline{\theta^2}$ , spatial variance  $\overline{y^2}$ , and covariance  $\overline{y\theta}$  (Eyges 1948, Hollmark *et al* 2004). Note that  $\overline{\theta^2}$ ,  $\overline{y\theta}$ ,  $\overline{y^2}$ , and  $T$  below are defined with projected positions and angles, amounting a half of those defined with radial positions and polar angles. As the particles receive energy loss and scattering in matter, the beam develops in space as

$$\overline{\theta^2}(x) = \int_0^x T(x') dx', \quad (7)$$

$$\overline{y\theta}(x) = \int_0^x (x - x') T(x') dx', \quad (8)$$

$$\overline{y^2}(x) = \int_0^x (x - x')^2 T(x') dx', \quad (9)$$

where scattering power  $T = d\overline{\theta^2}/dx$  is given by the multiple-scattering theory in use. The original theory and many subsequent applications use the Fermi-Rossi formula or effectively its variations for  $T$  without consideration of the single-scattering effect (Eyges 1948, Sandison *et al* 2000, Hollmark *et al* 2004) while some use the Highland formula for  $\overline{\theta^2}$  without explicit formulation of  $T$  (Kanematsu *et al* 1998, 2006, 2008b, Safai *et al* 2008).

## 2.2. Generalization for composite target

The Gottschalk form of the Highland formula (3) assumes  $X_0$  to be a unit for thickness  $x$  of a single homogeneous target. Often, however, a target may have a composite structure of multiple elements. The common practice to estimate the overall angular variance is application of the quadratic additivity rule  $\overline{\theta^2} = \sum_i \overline{\theta_i^2}$ , which may appear natural for independent scattering angles. It is, however, incompatible with the Highland formula. In the extreme case, if one divides the target into a great number of layers thinner than  $10^{-9} X_0$ , the Highland correction factor would be even negative.

Kanematsu *et al* (1998) addressed the ill-behaved logarithmic term by reinterpreting the parameters in (3), where  $x$  is redefined as the longitudinal position in the target,  $X_0$  is the radiation length varying with  $x$ , and  $\overline{\theta^2}$  is the angular variance growing with  $x$ . These reinterpretations slightly modify the formula to

$$\overline{\theta^2}(x) = \left(1 + \frac{1}{9} \lg \ell(x)\right)^2 \int_0^x \left(\frac{14.1 \text{ MeV } z}{pv(x')}\right)^2 \frac{dx'}{X_0(x')}, \quad (10)$$

where radiative path length  $\ell$  is defined as

$$\ell(x) = \int_0^x \frac{dx'}{X_0(x')}. \quad (11)$$

The generalized Highland formula (10) applies to the whole composite target to deal with medium heterogeneity in radiotherapy applications with special interest in the range of  $10^{-2} \lesssim \ell \lesssim 10^0$  corresponding to 0.0056–0.56 cm Pb, 0.089–8.9 cm Al, and 0.36–36 cm H<sub>2</sub>O (Yao *et al* 2006). In essence, the rms angle  $\sigma_\theta$  does not depend on geometrical placement, elementary composition, or density of the target elements, but only on the radiative path length  $\ell$ .

## 2.3. Differential Highland formula

The essence of the Highland formula (10) is the presence of the correction factor to the integral form of the Fermi-Rossi formula (2). It is natural to assume a similar correction factor  $f_H$  in the differential Highland formula

$$\frac{d\overline{\theta^2}}{dx} = f_H(\ell) \frac{1}{2} \left(\frac{E_s z}{pv}\right)^2 \frac{1}{X_0} \quad (12)$$

for the Gaussian scattering power with correction for the single-scattering effect. The average of the instantaneous correction factor for the radiative path length should coincide with the original Highland correction factor,

$$\frac{1}{\ell} \int_0^\ell f_H(\ell') d\ell' = \left(1 + \frac{\lg \ell}{9}\right)^2 \left(\frac{14.1 \text{ MeV}}{E_s/\sqrt{2}}\right)^2, \quad (13)$$

which leads the instantaneous correction factor to

$$\begin{aligned} f_H(\ell) &= \left(\frac{14.1 \text{ MeV}}{E_s/\sqrt{2}}\right)^2 \frac{d}{d\ell} \left[ \left(1 + \frac{\lg \ell}{9}\right)^2 \ell \right] \\ &= \left(\frac{14.1 \text{ MeV}}{E_s/\sqrt{2}}\right)^2 \left(1 + \frac{\lg \ell}{9}\right) \left(1 + \frac{2}{9 \ln 10} + \frac{\lg \ell}{9}\right) \\ &\approx 0.970 \left(1 + \frac{\ln \ell}{20.7}\right) \left(1 + \frac{\ln \ell}{22.7}\right). \end{aligned} \quad (14)$$

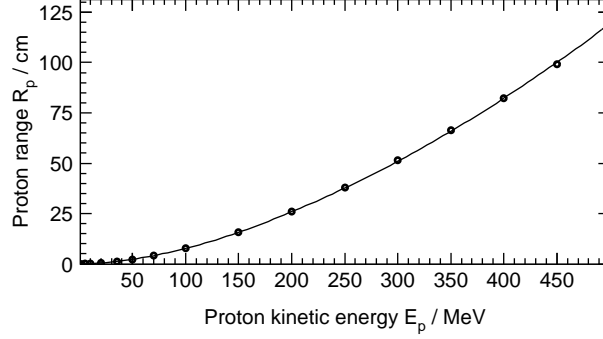


**Figure 2.** Range–energy relation curve in (17) with new parameters in (19) for protons in water with the ICRU (1993) data points.

#### 2.4. Range–energy relation

For convenience, kinetic energy  $E$  and position  $x$  are converted to residual range  $R$  and depth  $d$  expected in water that is the reference material in radiotherapy, by

$$R(E) = \int_0^E \frac{dE'}{S_w}, \quad d(x) = \int_{x_0}^x \frac{S}{S_w} dx' \simeq \int_{x_0}^x \rho_S dx', \quad (15)$$

where  $x_0$  is the incident point of the beam with energy  $E_0$  and residual range  $R_0$ . Usually, the beam range in water  $R_0$  is the only measurable quantity and residual ranges and energies are estimated from calculated depths as

$$R = R_0 - d, \quad E = E(R), \quad (16)$$

for which a predefined  $R$ – $E$  relation may be used. Bortfeld (1997) fitted the tabulated proton range–energy relation in water ( $R_p$ – $E_p$ ) by ICRU (1993) to power-law function

$$\frac{R_p}{\text{cm}} = \alpha \left( \frac{E_p}{\text{MeV}} \right)^\beta \quad \text{or} \quad \frac{E_p}{\text{MeV}} = \left( \frac{1}{\alpha} \frac{R_p}{\text{cm}} \right)^{1/\beta} \quad (17)$$

for proton energy  $E_p \leq 250$  MeV. This leads the  $R$ – $E$  relation for ions with charge  $ze$  and mass  $m = Au$  to

$$z^2 \frac{m_p}{m} \frac{R}{\text{cm}} = \alpha \left( \frac{m_p}{m} \frac{E}{\text{MeV}} \right)^\beta \quad (18)$$

because of  $R \propto E/S \propto m/z^2$  when  $E/m$  or  $v^2$  is fixed in (4), where  $e$  is the proton charge,  $u$  is the atomic mass unit, and  $m_p = 1.0073u$  is the proton mass. For fully stripped carbon ions or  $^{12}\text{C}$  nuclei, energy up to  $E/A \approx 400$  MeV is clinically necessary and we extend the  $R$ – $E$  relation with

$$(\alpha, \beta) = \begin{cases} (0.002441, 1.750) & \text{for } \frac{m_p}{m} \frac{E}{\text{MeV}} \leq 200 \\ (0.003849, 1.664) & \text{for } 200 < \frac{m_p}{m} \frac{E}{\text{MeV}} \lesssim 400, \end{cases} \quad (19)$$

which were determined with ICRU (1993) data points  $(E_p, R_p) = (100 \text{ MeV}, 7.718 \text{ cm})$  and  $(200 \text{ MeV}, 25.96 \text{ cm})$  for the first segment and  $(200 \text{ MeV}, 25.96 \text{ cm})$  and  $(400 \text{ MeV}, 82.25 \text{ cm})$  for the second segment. The deviations from the standard data are within either 0.1 cm or 1% for 0–400 MeV as shown in figure 2.

## 2.5. Beam development

The beam development in the Fermi-Eyges theory is computed in a stepwise manner to deal with variations of particle kinematics and medium heterogeneity. In small step  $\Delta x$  from  $x$ , the residual range and the radiative path length are modified by

$$\Delta R = -\rho_S(x) \Delta x, \quad \Delta \ell = \frac{\Delta x}{X_0(x)}, \quad (20)$$

and integrals (7)–(9) for the phase-space parameters are translated into

$$\Delta \overline{\theta^2} = \tilde{T} \Delta x, \quad (21)$$

$$\Delta \overline{y\theta} = \left( \overline{\theta^2} + \frac{\tilde{T}}{2} \Delta x \right) \Delta x, \quad (22)$$

$$\Delta \overline{y^2} = \left[ 2 \overline{y\theta} + \left( \overline{\theta^2} + \frac{\tilde{T}}{3} \Delta x \right) \Delta x \right] \Delta x, \quad (23)$$

where  $\tilde{T}$  is the effective scattering power for the step given by

$$\tilde{T} = f_H(\ell + \Delta \ell) \frac{E_s^2 z^2}{2 p v(x) p v(x + \Delta x) X_0(x)}, \quad (24)$$

with geometric-mean correction for  $p v$  variation in the step, which is accurate for steps within 20% of the residual range (Gottschalk *et al* 1993). Range uncertainty of for body tissue is usually 1% or more (Kanematsu *et al* 2003), which may limit the infimum for the step. Depth step  $\rho_S \Delta x$  may be controlled to be more than 0.5% of the initial range  $R_0$  and less than 10% of the residual range  $R$  by

$$\Delta x = \begin{cases} \min \left( \delta, \max \left( \frac{0.005 R_0}{\rho_S}, \frac{0.1 R}{\rho_S} \right) \right) & \text{for } R > 0.01 R_0 \\ R / \rho_S & \text{for } R \leq 0.01 R_0, \end{cases} \quad (25)$$

where  $\delta$  is the distance to the next density-voxel boundary in the presence of heterogeneity.

For the last step  $\Delta x = R / \rho_S$ , scattering power  $\tilde{T}$  would diverge due to the  $1/pv$  factor in (24) and incidentally angle  $\theta$  loses its physical significance at the end point. On the other hand, displacement  $y$  increases its importance for the Bragg peak and the last-step growth  $\Delta \overline{y^2}$  can be analytically calculated with (9), (12), (18), low-energy ( $E \lesssim m c^2$ ) approximation

$$\frac{1}{p^2 v^2} \approx \frac{1}{4 E^2} + \frac{1}{4 m c^2 E} - \frac{1}{18 m^2 c^4}, \quad (26)$$

and parameter conversion  $x \rightarrow (R_0 - R) / \rho_S$  as

$$\begin{aligned} \Delta \overline{y^2} &= \int_{\frac{R_0}{\rho_S} - \Delta x}^{\frac{R_0}{\rho_S}} \left( \frac{R_0}{\rho_S} - x' \right)^2 T(x') dx' = \frac{1}{\rho_S^3} \int_0^R R'^2 T(R') dR' \\ &= \frac{f_H}{8 X_0} \left( \frac{E_s z}{\text{MeV}} \frac{m_p}{m} \right)^2 \left( \frac{R}{\rho_S} \right)^3 \\ &\quad \times \left[ \frac{1}{3 - \frac{2}{\beta}} \left( \frac{m_p}{m} \frac{z^2 R}{\alpha \text{ cm}} \right)^{-\frac{2}{\beta}} + \frac{1}{3 - \frac{1}{\beta}} \frac{\text{MeV}}{m_p c^2} \left( \frac{m_p}{m} \frac{z^2 R}{\alpha \text{ cm}} \right)^{-\frac{1}{\beta}} - \frac{2}{27} \frac{\text{MeV}^2}{m_p^2 c^4} \right] \end{aligned} \quad (27)$$

with  $(\alpha, \beta) = (0.002441, 1.750)$ .

### 2.6. Semi-analytic formulation

The last-step growth  $\Delta\overline{y^2}$  can be extended in the other perspective, where particles with residual range  $R$  incident into homogeneous target receive multiple scattering until they stop at distance  $x = R/\rho_S$  with rms transverse displacement

$$\begin{aligned} \sigma_y(R) = & \left( 1 + \frac{1}{9} \lg \frac{R}{\rho_S X_0} \right) \frac{14.1}{2\sqrt{X_0}} \left( \frac{R}{\rho_S} \right)^{\frac{3}{2}} \left[ \frac{1}{3 - \frac{2}{\beta}} \left( \frac{R}{\alpha \text{ cm}} \right)^{-\frac{2}{\beta}} z^{2 - \frac{4}{\beta}} \left( \frac{m}{m_p} \right)^{\frac{2}{\beta} - 2} \right. \\ & \left. + \frac{1}{3 - \frac{1}{\beta}} \frac{\text{MeV}}{m_p c^2} \left( \frac{R}{\alpha \text{ cm}} \right)^{-\frac{1}{\beta}} z^{2 - \frac{2}{\beta}} \left( \frac{m}{m_p} \right)^{\frac{1}{\beta} - 2} - \frac{2}{27} \frac{\text{MeV}^2}{m_p^2 c^4} z^2 \left( \frac{m}{m_p} \right)^{-2} \right]^{\frac{1}{2}}, \quad (28) \end{aligned}$$

where correction factor  $f_H$  in (27) has been restored to the original form for radiative path length  $R/(\rho_S X_0)$  in analogy with (13).

Incidentally, Hong *et al* (1996) found almost linear relation between  $\sigma_y$  and  $R$  for protons in water, with fitted function

$$\sigma_{y_p}(R) = 0.02275 R + 0.12085 \times 10^{-4} R^2 / \text{cm}, \quad (29)$$

where the second term amounts within 2% for  $R \lesssim 40$  cm and may be negligible. The linear approximation greatly simplifies the range-dependent factor in (28), while the material-dependent factor and the projectile-dependent factor scale predominantly with  $1/\sqrt{(\rho_S^3 X_0)}$  and  $z^{1-2/\beta} (m/m_p)^{1/\beta-1}$ , leading to

$$\sigma_y(R) = F_{zA} \sqrt{\frac{X_{0w}}{\rho_S X_0} \frac{R}{\rho_S}}, \quad (30)$$

$$F_{zA} = \frac{d\sigma_{y_p}}{dR} z^{1-\frac{2}{\beta}} \left( \frac{A u}{m_p} \right)^{\frac{1}{\beta}-1} = 0.02282 z^{-0.1429} A^{-0.4286}, \quad (31)$$

where  $X_{0w} = 36.08$  cm is the radiation length of water. The linear  $\sigma_y(R)$  formula (30) is comprised of the projectile factor  $F_{zA}$ , square-root of the scattering/stopping ratio  $(\frac{T}{S})/(\frac{T}{S})_w = X_{0w}/(\rho_S X_0)$ , and the geometrical range  $R/\rho_S$ .

Differentiation of (9) in conjunction with (30),  $R = R_0 - \rho_S x$ , and  $\sigma_y^2 = \overline{y^2}$  leads to scattering power

$$T(R) = \frac{\rho_S^3}{R^2} \frac{d\sigma_y^2}{dR} \simeq 2 F_{zA}^2 \frac{X_{0w}}{X_0} \frac{\rho_S}{R}, \quad (32)$$

which is put back in (9) to give spatial variance

$$\begin{aligned} \overline{y^2}(x) &= 2 F_{zA}^2 \frac{X_{0w}}{X_0} \int_{R_0 - \rho_S x}^{R_0} \frac{(R' + \rho_S x - R_0)^2}{\rho_S^2 R'} dR' \\ &= F_{zA}^2 \frac{X_{0w}}{X_0} \left[ 3x^2 - 2 \frac{R_0}{\rho_S} x + 2 \left( \frac{R_0}{\rho_S} - x \right)^2 \ln \frac{R_0}{R_0 - \rho_S x} \right] \quad (33) \end{aligned}$$

at any position  $x$ . This reduces to a very universal formula for relative growth of the rms displacement,

$$\frac{\sigma_y(x_R)}{\sigma_y(x_R = 1)} = \sqrt{3x_R^2 - 2x_R - 2(1-x_R)^2 \ln(1-x_R)}, \quad (34)$$

where  $x_R = \rho_S x/R_0$  is the range-normalized distance in  $[0, 1]$  and  $\sigma_y(x_R = 1)$  is the end-point rms displacement or  $\sigma_y(R = R_0)$  in (30). In fact, the universal formula (34) seemed to be known by Preston and Koehler of Harvard Cyclotron Laboratory by year 1968 for protons of any energy incident into any homogeneous material.



**Table 1.** Atomic properties (mass density, mass-electron density, mean excitation energy, radiation mass length, and mass-stopping-power ratio at  $v^2 = 0.5 c^2$ ) of water and target materials.

Material	$\rho/\frac{\text{g}}{\text{cm}^3}$	$\frac{n_e}{\rho N_A}/\frac{\text{mol}}{\text{g}}$	$I/\text{eV}$	$\rho X_0/\frac{\text{g}}{\text{cm}^2}$	$\frac{\rho_S}{\rho}/\frac{\text{cm}^2}{\text{g}}$
Water	1	0.5551	75	36.08	1
Beryllium	1.85	0.4438	63.7	65.19	0.8141
Copper	8.96	0.4564	322	12.86	0.6894
Lead	11.35	0.3958	823	6.37	0.5236

### 2.7. Application and validation

This study addresses formulation and implementation of the Highland's correction for the scattering power in the Fermi-Eyges theory that is generally applicable to heterogeneous system, and presents approximate formulas for the rms transverse displacement in homogeneous system. We here examine consistencies and differences of the present formulation against other studies.

*2.7.1. Range and scattering angle* Range estimation with (18) and (5) and the rms angles by numerical computation in section 2.5 were examined against reference data by Gottschalk *et al* (1993) for 158.6 MeV protons incident into beryllium, copper, and lead targets with properties in table 1.

*2.7.2. Transverse displacement* The rms transverse displacements  $\sigma_y = \sqrt{\langle y^2 \rangle}$  in water ( $\rho_S = 1$ ,  $X_0 = 36.08$  cm) were calculated as a function of depth  $x$  for projectile nuclei  $R = 29.4$  cm  $^1\text{H}$ , 29.4-cm  $^4\text{He}$ , and 29.7-cm  $^{12}\text{C}$  to compare with Phillips's measurements (Hollmark *et al* 2004) and with the universal formula (34).

*2.7.3. End-point displacement* The rms transverse displacement at the end point,  $\sigma_y(R)$ , of nuclei  $^1\text{H}$ ,  $^4\text{He}$ , and  $^{12}\text{C}$  incident into water were calculated for varied incident energies and were compared with the analytical (28) and the linear (30) formulas, and with Hong's curve (29) for protons.

*2.7.4. Heterogeneity handling* We examined the end-point rms displacement  $\sigma_y(R)$  of  $R = 29.4$  cm protons in a target comprised of alternative high (1.1) and low (0.9) density equal-thickness layers of water. The end-point rms displacements were calculated by numerical Fermi-Eyges integrals using the differential Highland formula (12) and, for comparison, using the Fermi-Rossi formula (2) or the effective scattering power per layer individually calculated with the Highland-Gottschalk formula (3)

$$\tilde{T}_i = \left(1 + \frac{1}{9} \lg \frac{t}{\rho_i X_{0w}}\right)^2 \int_0^t \left(\frac{14.1 \text{ MeV}}{pv(x_i + dt')}\right)^2 \frac{dt'/t}{\rho_i X_{0w}}, \quad (35)$$

where  $\rho_i = \{1.1, 0.9, 1.1, 0.9, \dots\}$  and  $x_i = \{0, t, 2t, \dots\}$  are the relative density and the start position of layer  $i$ , and  $t$  is the layer thickness varied in the range of 0.01–1 cm.

**Table 2.** 158.6-MeV proton mass ranges estimated ( $R_p\rho/\rho_S$ ) and computed ( $\rho\int_0^{E_p} dE/S$ ) and rms angles calculated with the Fermi-Rossi ( $\theta_{FR}$ ), the Highland-Gottschalk ( $\theta_{HG}$ ), and the differential Highland ( $\theta_{dH}$ ) formulas with the Molière-Hanson angles ( $\theta_{MH}$ ) calculated by Gottschalk *et al* (1993) at range-normalized thicknesses  $x_R = 1\%$  and  $10\%$  of beryllium, copper, and lead targets.

	Beryllium		Copper		Lead	
$(R_p\rho/\rho_S)/\frac{g}{cm^2}$	21.25		25.10		33.04	
$(\rho\int_0^{E_p} dE/S)/\frac{g}{cm^2}$	21.11		25.92		35.21	
$x_R$	1%	10%	1%	10%	1%	10%
$\theta_{FR}/\text{mrad}$	2.92	9.46	7.21	23.38	11.84	38.43
$\theta_{HG}/\text{mrad}$	1.98	7.42	5.49	20.26	9.56	35.04
$\theta_{dH}/\text{mrad}$	2.03	7.58	5.61	20.65	9.75	35.69
$\theta_{MH}/\text{mrad}$	2.01	7.17	5.63	20.40	9.75	35.76

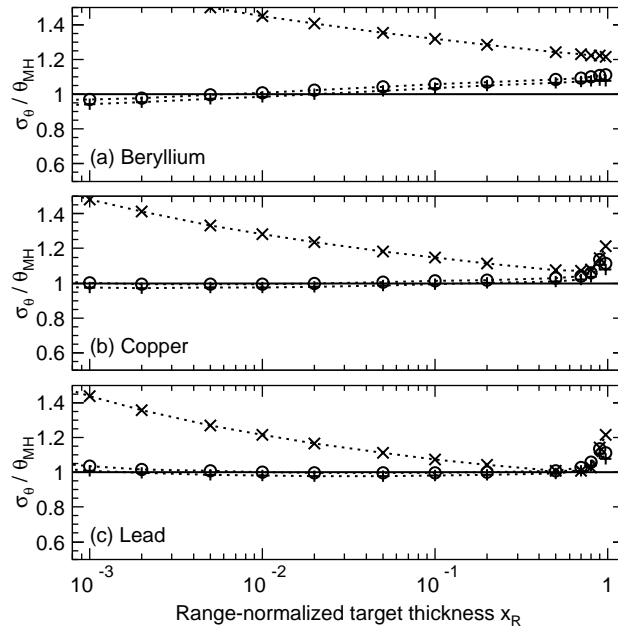


**Figure 3.** Relative rms angles of the Fermi-Rossi ( $\sigma_\theta = \theta_{FR}$ , symbol  $\times$ ), the Highland-Gottschalk ( $\sigma_\theta = \theta_{HG}$ , symbol  $+$ ), and the differential Highland ( $\sigma_\theta = \theta_{dH}$ , symbol  $\circ$ ) formulas with respect to the Molière-Hanson angles  $\theta_{MH}$  (zero level) by Gottschalk *et al* (1993) for 158.6 MeV protons in (a) beryllium, (b) copper, and (c) lead targets as a function of target thickness.

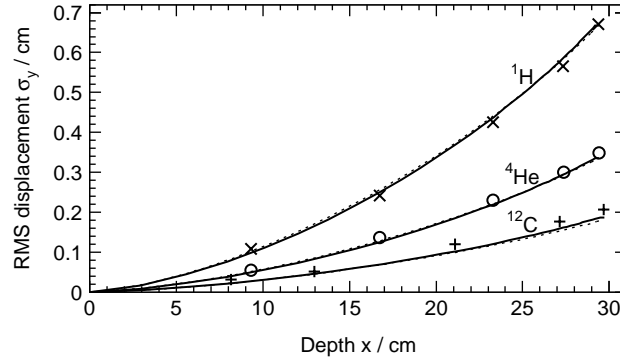


**Figure 4.** Rms transverse displacements in water for projectile nuclei  $R = 29.4$  cm  $^1\text{H}$ ,  $29.4$ -cm  $^4\text{He}$ , and  $29.7$ -cm  $^{12}\text{C}$  as a function of depth, calculated by the numerical computation (solid) and the universal formula (34) (dotted). Markers indicate Phillips's measurements of  $1/e$  radius  $\sqrt{2}\sigma_y$  drawn by Hollmark *et al* (2004).

### 3. Results

#### 3.1. Range and scattering angle

Equation (18) leads the range of  $158.6$  MeV protons in water to  $R_p = 17.30$  cm. The mass ranges in beryllium, copper, and lead targets estimated by  $R_p \rho/\rho_S$  with semi-relativistic approximation (5) for  $\rho_S$  are compared to exact calculations  $\rho \int_0^{E_p} dE/S$  in table 2. The discrepancy was as large as 6% with lead for its very high  $I$  value. The rms scattering angles are compared in figure 3 and in table 2. The two Highland formulas equally corrected the single-scattering effect.

#### 3.2. Transverse displacement

Figure 4 shows the growths in transverse displacement of nuclei  $^1\text{H}$ ,  $^4\text{He}$ , and  $^{12}\text{C}$  in water. The present calculations made excellent agreement with the measurements by Phillips and with the universal  $\sigma_y(x_R)$  formula (34).

#### 3.3. End-point displacement

Figure 5 shows the rms displacements of nuclei  $^1\text{H}$ ,  $^4\text{He}$ , and  $^{12}\text{C}$  at the end point in water for varied incident energies. The numerical computation, the analytical (28) and the linear (30) formulas, and Hong's curve (29) were all in agreement within 2%.

#### 3.4. Heterogeneity handling

Figure 6 shows the behaviors of the formulations against the heterogeneity of the multilayered target. The layer-wise calculation of the Highland-Gottschalk angles (35) actually caused underestimation of the rms displacement as addressed in section 2.2. For a typical step size of  $0.1$  cm for heterogeneity handling, the error was  $-26\%$  with respect to the differential Highland formula, which was much worse than that of  $+12\%$  by the Fermi-Rossi formula.

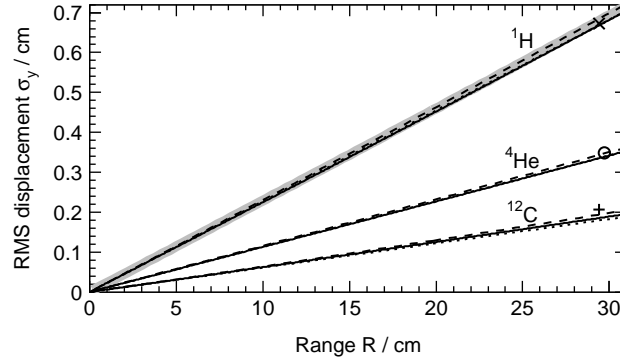


**Figure 5.** End-point rms transverse displacements in water for projectile nuclei  $^1\text{H}$ ,  $^4\text{He}$ , and  $^{12}\text{C}$  as a function of range  $R$ , by the numerical computation (solid), the analytical formula (28) (dashed), the linear formula (30) (dotted), and Hong's curve (29) for protons (thick light gray). Markers indicate Phillips's measurements.

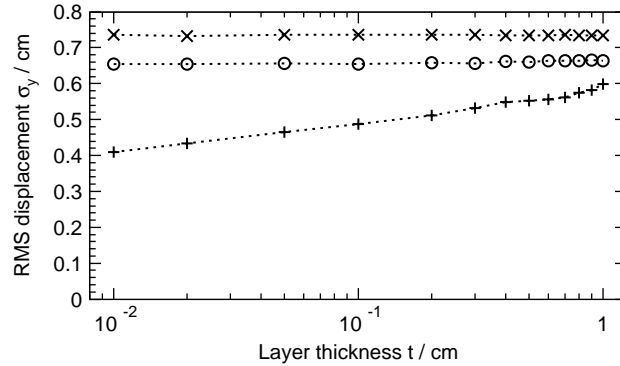


**Figure 6.** End-point rms transverse displacements of  $R = 29.4$  cm protons in alternatively layered high (1.1) and low (0.9) density water of varied layer thickness  $t$ , calculated with the Fermi-Rossi formula ( $\times$ ), the differential Highland formula ( $\circ$ ), and the Highland-Gottschalk formula individually applied to every layer ( $+$ ).

## 4. Discussion

### 4.1. Improvement in scattering formulation

The Fermi-Eyges theory smartly describes the development of a particle beam with a set of several beam-defining parameters by simple numerical path integrals. The scattering power drives the development, for which the Fermi-Rossi formula (2) or those without consideration of the single-scattering effect may not be very accurate as so found by Hollmark *et al* (2004) in comparison with Phillips's measurements. In dealing with fine heterogeneity, the original Highland formula misused for each layer (35) would cause substantial errors as shown in figure 6. It was just not designed to be used in such manner.

The modified Highland formulas presented in this work, the integral form (10)

and the differential form (12), are essentially equivalent. While the differential form gives the scattering power  $T$ , the integral form directly gives angular variance  $\overline{\theta^2}$  from which its increment per step  $\Delta\overline{\theta^2} = \overline{T}\Delta x$  will be derived. The framework has been validated for protons in the presence of heterogeneity against Monte Carlo simulations (Kanematsu *et al* 1998) and measurements (Akagi *et al* 2006).

It would be interesting to note that the concept of the scattering power involves contradiction in its definition  $T = d\overline{\theta^2}/dx$ . In the infinitesimal distance, there would be no multiple but at most a single scattering and the central limit theorem should be invalid. The scattering power should be merely a mathematical quantity for the convenience of formulation. However, if it is explicitly required in the Fermi-Eyges theory, the differential Highland formula will be the solution with consideration of the single-scattering effect.

#### 4.2. Assessment for radiotherapy

In radiotherapy, majority of energies are normally spent in human body or range adjustment devices made of tissue-like materials. When the beam range is fixed, the effect of the Highland correction may be reasonably constant. For  $R = 29.4$  cm protons in figure 6, the effective Highland correction factor to  $\sigma_y(R)$  of the Fermi-Rossi formula was 1/1.12. With reduction of the energy constant  $E_s/\sqrt{2} = 15.0$  MeV to 13.4 MeV, the Fermi-Rossi formula would be approximate to the Highland formula in this case. Incidentally, the energy constants were effectively  $E_s/\sqrt{2} \approx 13.1$  MeV by Sandison *et al* (2000) and  $E_s/\sqrt{2} \approx 14.3$  MeV by Hollmark *et al* (2004) with  $X_0 = 36.08$  cm for water. Those theoretical formulations have little experimental basis as compared to the Molière theory and its approximations (Gottschalk *et al* 1993).

For beam field formation, some metal scatterers and energy degraders are often used in beam-delivery systems. The scattering powers of those devices, often with complex structure, must be precisely controlled to deliver designed beams. For systems with small number of scattering elements with certain thicknesses, the original Highland formula and the quadratic-additivity rule may be reasonably valid (Hong *et al* 1996, Safai *et al* 2008). Since energy loss in the scatterers is usually marginal, the semi-relativistic approximation for the stopping-power ratio  $\rho_S$  in (5) should be valid even for heavy metals like lead.

The great advantage of the Fermi-Eyges theory is wide-ranged applicability. It can accurately and efficiently handle field formation in beam delivery systems, beam customization for individual treatment targets, and beam transport in patients to give a variable Gaussian kernel for dose calculation (Kanematsu *et al* 1998, 2006, 2008a, 2008b), all by simple path integrals. The present framework can handle the effect of multiple scattering at 1–2% level accuracy for displacements within 1 cm, which is sufficiently small and safe against the clinical tolerances typically of 1 mm.

Theory of range straggling that broaden the Bragg peak is also satisfactorily mature (Bortfeld 1997, Kanematsu *et al* 1998, Hollmark *et al* 2004) though nuclear interactions that degrade the Bragg peak and radiation quality with nuclear fragments have yet to be studied (Kameoka *et al* 2008). In practice, those effects are implicitly involved in measured or pre-calculated in-water depth–dose curves that are quickly referenced in dose calculation (Kanematsu *et al* 2008a).

### 4.3. Parametric formulas

Bortfeld's power-law formula (17) for proton  $R$ - $E$  relation has been generalized for ions in (18) to cover wider energies with two segments, which could be further extended with multiple segments if necessary. The relationship is based on the standard ICRU (1993) data calculated with  $I = 75$  eV for water. When the standard data change with an improved  $I$  value, parameter  $\alpha$  in (19) needs to change accordingly.

Generality and usability are merits of analytical formulation. The analytical  $\sigma_y(R)$  formula (28) for end-point rms displacement applies to any projectile nucleus in any homogeneous material as far as the  $R$ - $E$  relation is valid. Assuming the linearity between  $\sigma_y$  and  $R$ , the linear  $\sigma_y(R)$  formula (30) and the universal  $\sigma_y(x_R)$  formula (34) for growth with range-normalized distance  $x_R$  have been derived. The agreement among these formulations and measurement in figure 4 and figure 5 should have added extra credibility to this work.

## 5. Conclusions

The Gaussian scattering power with correction for single-scattering effects has been formulated, which can be used in the framework of the Fermi-Eyges theory for beam transport calculation in wide-ranged applications for radiotherapy with heavy charged particles. The numerical computation procedure will be robustly and efficiently applicable to heterogeneous systems, while semi-analytical formulas derived in the present study will be useful for estimation of scattering effects in homogeneous systems. Calculations for protons, helium ions, and carbon ions agreed with other experimental and theoretical studies at a level of 1–2% in scattering displacement of typically within 1 cm, which is satisfactory against typical clinical tolerance of 1 mm for high-precision radiotherapy.

## Acknowledgments

The author wish to thank Bernard Gottschalk for his self-published online materials on this matter that greatly helped this writing especially on the historical issues.

## References

- Akagi T, Kanematsu N, Takatani Y, Sakamoto H, Hishikawa Y and Abe M 2006 Scatter factors in proton therapy with a broad beam *Phys. Med. Biol.* **51** 1919–28
- Bichsel H 1958 Multiple scattering of protons *Phys. Rev.* **112** 182–5
- Bethe H A 1953 Molière's theory of multiple scattering *Phys. Rev.* **89** 1256–66
- Bortfeld T 1997 An analytical approximation of the Bragg curve for therapeutic proton beams *Med. Phys.* **24** 2024–33
- Chu W T, Ludewigt B A, and Renner T R 1993 Instrumentation for treatment of cancer using proton and light-ion beams *Rev. Sci. Instrum.* **64** 2055–122
- Cianguaru G, Polf J C, Bues M and Smith A R. 2005 Benchmarking analytical calculations of proton doses in heterogeneous matter *Med. Phys.* **32** 3511–23
- Deasy J O 1998 A proton dose calculation algorithm for conformal therapy simulations based on Molière's theory of lateral deflections *Med. Phys.* **25** 476–83
- Eyges L 1948 Multiple scattering with energy loss *Rhys. Rev.* **74** 1534–5
- Gottschalk B, Koehler A M, Schneider R J, Sisterson J M and Wagner M S 1993 Multiple Coulomb scattering of 160 MeV protons *Nucl. Instr. Methods Phys. Res. B* **74** 467–90
- Hanson A O, Lanzl L H, Lyman E M and Scott M B 1951 Measurement of multiple scattering of 15.7-MeV electrons *Phys. Rev.* **84** 634–7
- Highland V L 1975 Some practical remarks on multiple scattering *Nucl. Instr. Methods.* **129** 497–9

- Hollmark M, Uhrdin J, Dž B, Gudowska I and Brahme A 2004 Influence of multiple scattering and energy loss straggling on the absorbed dose distributions of therapeutic light ion beams: I. Analytical pencil beam model *Phys. Med. Biol.* **49** 3247–65
- Hong L, Goitein M, Bucciolini M, Comiskey R, Gottschalk B, Rosenthal S, Serago C and Urie M 1996 A proton beam algorithm for proton dose calculations *Phys. Med. Biol.* **41** 1305–30
- ICRU 1993 Stopping powers and ranges for protons and alpha particles *International Commission on Radiation Units and Measurements Report 49* (Bethesda, MD: ICRU)
- Kameoka S *et al* 2008 Dosimetric evaluation of nuclear interaction models in the Geant4 Monte Carlo simulation toolkit for carbon-ion radiotherapy *Radiol. Phys. Tech.* (in press).
- Kanematsu N, Akagi T, Futami Y, Higashi A, Kanai T, Matsufuji N, Tomura H and Yamashita H 1998 A proton dose calculation code for treatment planning based on the pencil beam algorithm *Jpn. J. Med. Phys.* **18** 88–103
- Kanematsu N, Matsufuji N, Kohno R, Minohara S and Kanai T 2003 A CT calibration method based on the polybinary tissue model for radiotherapy treatment planning *Phys. Med. Biol.* **48** 1053–64
- Kanematsu N, Akagi T, Takatani Y, Yonai S, Sakamoto H and Yamashita H 2006 Extended collimator model for pencil-beam dose calculation in proton radiotherapy *Phys. Med. Biol.* **51** 4807–17
- Kanematsu N, Yonai S and Ishizaki A 2008a The grid-dose-spreading algorithm for dose distribution calculation in heavy charged particle radiotherapy *Med. Phys.* **35** 602–8
- Kanematsu N, Yonai S, Ishizaki A and Torikoshi M 2008b Computational modeling of beam-customization devices for heavy-charged-particle radiotherapy *Phys. Med. Biol.* **53** 3113–3127
- Rutherford E 1911 The scattering of  $\alpha$  and  $\beta$  particles by matter and the structure of the atom *Philosophical Magazine Series 6* **21** 669–88
- Rossi B and Greisen K 1941 Cosmic ray theory *Rev. Mod. Phys.* **13** 240–309
- Safai S, Bortfeld T and Engelsman M 2008 Comparison between the lateral penumbra of a collimated double-scattered beam and uncollimated scanning beam in proton radiotherapy *Phys. Med. Biol.* **53** 1729–50
- Sandison G A and Chvetsov A V 2000 Proton loss model for therapeutic beam dose calculations *Med. Phys.* **27** 2133–45
- Wong M, Schimmerling W, Phillips M H, Ledewigt B A, Landis D A, Walton J T and Curtis S B. *Med. Phys.* **17** 163–71
- Yao W M, *et al* (Particle Data Group) 2006 *J. Phys. G* **33** 1–1232